The Semi-Coaxial Multirotor

Dmitry Bershadsky
Post-Doctoral Researcher
Georgia Institute of Technology
Atlanta, GA, USA

Stephen Haviland
Graduate Research Assistant
Georgia Institute of Technology
Atlanta, GA, USA

Eric N. Johnson
Professor of Aerospace Engineering
Pennsylvania State University
State College, PA, USA

ABSTRACT

The "semi-coaxial" multirotor configuration is presented including its advantages over the conventional coaxial rotor configuration. The semi-coaxial configuration retains the benefits of the coaxial configuration, and additionally alleviates the loss of efficiency encountered when rotors are stacked coaxially. In addition to being more power-efficient than the standard coaxial configuration, the described configuration allows for nearly- or fully-actuated control of a multirotor when used in configurations such as the three-armed *Y6* hexarotor. Using this configuration, a new Direct Force Control (DFC) multirotor is presented: the *Y6sC*, a specific example of the semi-coaxial multirotor. The configuration orients six rotors in a way which allows the vehicle to hover in non-zero attitudes and translate without rotating with higher efficiency than the corresponding coaxial design.

INTRODUCTION

In recent years, as multirotors have become more capable, there has been more attention paid in research to increasing the degrees of freedom (DOF). As these designs mature, it becomes more valuable to increase their efficiency. This paper describes the design, efficiency, and control authority of a novel vehicle. The design builds on existing research on direct force control (DFC) and an existing multirotor design, the so-called *Y6*.

Fig. 1. Net rotor thrust for a conventional, planar multirotor (1) versus *Y6sC* (2) in moving to a new desired position (x_{des}). Regions A-C are at different times during the maneuver where the arrows indicate the force vector.

In Mulgaonkar (Ref. 1), a study was completed on how maneuverability changed with the scale of the multirotor. As the scale of the vehicle became smaller both translational and rotational acceleration increased; smaller multirotors are more maneuverable than their larger counterparts. Conventional multirotors are underactuated: they have direct access to four degrees of freedom, i.e, pitch, roll, yaw, and "up." They are not capable of generating instantaneous translational and/or rotational acceleration in any arbitrary direction, namely fore/aft, left/right. This is due to all rotors being aligned (i.e., coplanar). For a standard planar multirotor to move from one position to another, as seen in Figure 1, the vehicle is required to change its orientation by applying a torque. This allows part of the total thrust vector to point horizontally allowing the vehicle to move in its commanded direction. Higher DOF designs such as the one described hereinafter can generate force in the horizontal plane without rotating. This allows the vehicle to more quickly accelerate as seen in block *A*. The direct force design in this paper has only fractional amount of force capability compared to the vertical direction. As such, a conventional multirotor can generate more horizontal acceleration by tilting as seen in block *B*, if necessary. During the deceleration phase (block *C*), the planar multirotor has to more aggressively retard its motion compared to the higher-DOF design. The higher-DOF vehicle thus has a higher bandwidth for position hold when small or high-frequency corrections are needed. Another benefit of a higher-DOF design is that it can fly the same maneuver shown at a constant non-level attitude. If the vehicle was required to point in a specific direction it could maintain the orientation throughout the trajectory. Such a vehicle can also hover at non-zero attitudes, unlike its conventional counterpart.

DFC vehicles are generally flown with the detriment of sacrificing hover efficiency for DFC. Several studies have been written regarding development of non-conventional designs and uses of multirotors. Augugliaro (Ref. 2) describes building tensile structures in difficult to access places. Mellinger (Ref. 3) describes aerial grasping control, estimation, and relevant mechanical design. Fumagalli (Ref. 4) develops a model for interaction with the environment of a multirotor using a compliant manipulator. Gioioso (Ref. 5) performs a stability analysis of different interaction tasks. Yuksel (Ref. 6) provides a force observer for these tasks as well. A company is also investigating using DFC to perform the tedious task of cleaning windows and solar panels for large buildings and arrays (Ref. 7).

Jiang (Ref. 8) claims another benefit for DFC: faster disturbance rejection than a standard vehicle. Because the vehicle has direct access to produce small forces in the direction of the

Presented at the AHS International 74th Annual Forum & Technology Display, Phoenix, Arizona, USA, May 14–17, 2018.

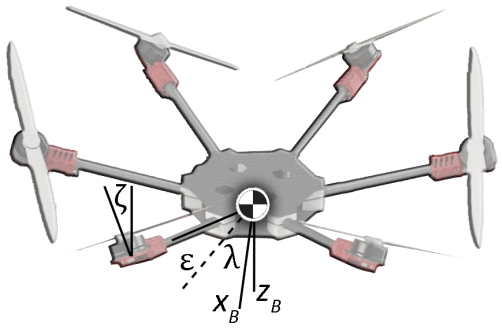

Fig. 2. DFC design variables on an *X6* : motor tilt ζ, arm dihedral ε, and arm azimuth λ

disturbance, it is shown that the vehicle is capable of quicker responses to these, without having to reorient itself to do so. Jiang (Ref. 9) also describes a vehicle utilizing DFC to swab an exhaust shaft at a power facility. The same authors also performs an optimization study for the orientation of rotors from 0-35° of motor roll about the arm (referred to as ζ herinafter). There is no treatment of negative ζ or any dihedral, or any other vehicle types.

More extreme DFC designs have also been investigated. Crowther (Ref. 10), Jiang (Ref. 11), Kaufman (Ref. 12), Rajappa (Ref. 13), and Nikou (Ref. 14) also describe non-coplanar multirotor designs which can actuate in 6 DOF. Brescianini (Ref. 15) describes the design and modeling of a vehicle capable of a true 6 DOF actuation configuration. In the study, the author optimizes the orientations of 6 and 8 rotor vehicle, with positions pinned to particular polyhedra. They built and flew a cube vehicle providing flight results for a vehicle with 8 reversible rotors. They use a simplified force, torque model and are not able to fully decouple translational and rotational dynamics. The cube design can fly in any arbitrary orientation due to its symmetry, but it is on the more inefficient side of hover power in these attitudes due to the rotors facing in multiple, more independent directions away from "down." That is, if rotors aren't used for hover in a particular attitude, they merely become payload. The author also shows the vehicle catching a ball thrown inside a controlled environment. Nikou (Ref. 14) designs a heptarotor using an optimizer. The structure and rotor positioning and orientation is arbitrary, so this is likely a more extreme example of DFC optimization leading to hover inefficiency. Park (Ref. 16) describes the design, modeling and control of yet another omni-directional vehicle with nearly arbitrary positioning and orientations on a pole. This study also proposes a reversible rotor by stacking two of the same propeller on the shaft and using reversible ESCs. This, the author claims, allows for a gain of actuator authority for a marginal loss of efficiency. Kiso (Ref. 17) considers optimization of a constant inertia vehicle with no rotor dynamics. Only counter-rotating coaxial rotors with no wake-wake interference or arm dihedral are considered and the metric of "manipulability" is introduced.

Aerodynamics of these small vehicles at low Reynolds numbers (on the orders of 10,000 - 100,000) are becoming of interest as modeling becomes more detailed and optimization becomes more important. Markusic (Ref. 18) describes a thrust stand for electric rotor evaluation. Many designs exist but this design is of interest to the study described by this work. Rand (Ref. 19) describes an optimization technique for stacking coaxial rotors and use of BEMT modeling techniques in hover and axial flight. Leishman (Ref. 20) describes the same with further detail and introduces the optimum coaxial rotor system. For oblique flow, Theys (Ref. 21) describes experiments comparing BEMT calculations and observations made in a wind tunnel for a low Reynolds number rotor, such as the ones considered in this thesis. In that study, it is stated that BEMT fails to predict performance at these angles. Theys proposes a correction factor factor for these less-axial inflow conditions. Otsuka (Ref. 22) studies some of the aspects of multirotor aerodynamics of interest in this study. In it, they propose a design with partially overlapping blades, much like existing designs such as the CH-47. This design's main advantage over a standard *X8* is to save lateral size by partially overlapping the rotors. There is a reduction in hover efficiency of course due to wake-rotor interaction, which is studied for this configuration. Tip to tip distance is also studied and found to not be a factor affecting efficiency (although this is contradicted by Alexandrov (Ref. 23), who claims that there is an optimal gap distance for multirotors). Counter-rotating rotors only are described in that study, and no wake effects at oblique angles are considered, nor is mechanical power or efficiency.

This paper describes a new rotor configuration which inspired the design of the *Y6sC*, a new multirotor configuration. The *Y6sC* optimizer is referenced and is used to model the design; optimization is out of scope for this paper, see (Ref. 24) for more details. The design is compared to the conventional *Y6C*. Thrust stand results of the rotor configuration are provided (both co-rotating and counter-rotating rotors), along with a sensitivity study on the angle of motor tilt (ζ) from the conventional coaxial configuration. Finally, flight test results are shown for the initial prototype *Y6sC*, which allows for easy modification of ζ. Data for the rotor out case is also described along with the controller used for the prototype.

Contributions

The contributions of the semi-coaxial configuration presented in this paper include the following:

- Semi-coaxial is more efficient than pure coaxial in hover in general
- Semi-coaxial rotor configuration allows for DFC capability on the conventional *Y6C* with no loss and possible gain in hover efficiency when converted to *Y6sC*
- *Y6sC* authority data are provided considering arm dihedral and motor tilt, including rotor out
- Thrust stand data are provided for semi-coaxial configuration using co- and counter-rotating rotors

- Motor-out cases of the *Y6sC* are more fault-tolerant than of the *Y6C*
- Maximum rates of the *Y6sC* are around 1-5% higher than those of the *Y6C*
- Flight tests performed to validate the proposed benefits

NEW *Y6SC* DESIGN

DFC simulation and optimization

To investigate the control authority of these vehicles, a framework was developed to study how configuration changes affect rate generation capability (i.e., actuation authority) in the 6 DOF. Multirotor dynamics are developed and used to calculate these for a multitude of motor tilt angles ζ and arm dihedral angles ε. An example output surface is shown in Figure 5, which shows pure motion authority in the x_B direction; that is, the sensitivity to the maximum instantaneous acceleration the vehicle can produce in that direction with non-coupled motion (i.e., no acceleration in roll, pitch, yaw, or in the y_B or z_B directions). Impure motion is also studied and is a less computationally intensive case. Simulation of a controller is needed to provide motor commands for generating the authority envelopes. A sequential quadratic programming (SQP) approach is used to create a controller to check for the maximum rate capability while maintaining a pure motion constraint.

An optimizer is placed on top of this in order to automatically design these types of vehicles. The optimizer developed takes user defined constraints (e.g., design variables and limits) and goals (e.g., maximize acceleration in the x_B and y_B directions) and outputs the optimal rotor configuration. More details can be found in (Ref. 24). To investigate the rotor out scenario, the framework is also capable of disabling rotors. Actuation authority surfaces for these scenarios are also available in the reference.

Y6sC design

One type of conventional hexarotor is the *Y6C* is shown in Figure 3 (a). Although the *Y6C* has the advantage of lower inertia and potentially lower physical complexity than the *X6* (Figure 4), it is not directly capable of DFC in the x_B and y_B axes, and suffers coaxial rotor losses. The presented modification to this design is termed the *Y6sC*, where the "s" indicates "semi-coaxial." The design is shown in Figure 3 (c), where the downstream (lower) rotors are mounted at the negative of the ζ of the upstream (top) rotors. One advantage of the design is a *gain of two DOF for only a reorientation of the same propulsion system.* Another advantage of this design is the airflow from the upstream to the downstream rotor is not perpendicular to the downstream rotor's plane. This is advantageous in that the downstream rotor does not ingest the full wash of the upstream rotor, which should act to decrease the loss of efficiency of this stacked configuration. This is in opposition to the *Y6C* when ζ is applied, seen in Figure 3 (b), where the same angle is applied such that the rotors stay coaxial. The *Y6sC* design has not been described or flown in literature.

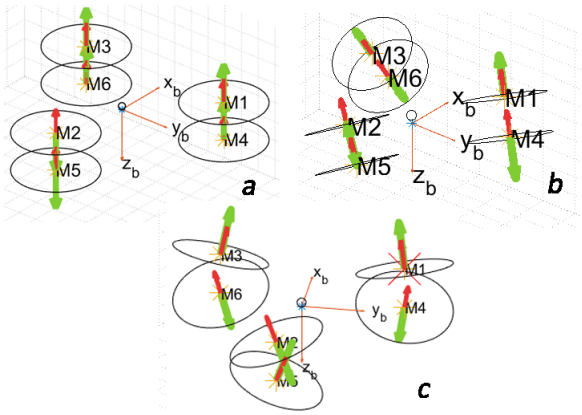

Fig. 3. *Y6* counter-rotating configurations: (a) conventional *Y6C* (ζ = 0°), (b) *Y6C* (ζ = 20°), (c) *Y6sC* (ζ = 20°). Green vectors indicate spin direction, red vectors indicate force direction.

Fig. 4. *Y6sC* prototype, ζ = 30°

X6* and *Y6C* vs. the novel *Y6sC One downside of the *Y6sC* is the height of the mount (the distance from the seat of the motor to the arm) scales with ζ to avoid propeller strikes between the top and bottom rotors. However, this design gains some of the advantages seen by the *X6*, and at a generally lower inertia cost if the motor mounts are light. The main advantage of the *Y6sC* over the *Y6C* is the gained ability to generate acceleration in the x_B and y_B axes. The conventional *Y6C* cannot achieve this authority without adding dihedral or motor tilt ζ (where the rotors remain coaxial) or some other motor reorientation. Table 1 shows the differences in maximum rates (impure) in the angular directions. Note that the *Y6sC* is also faster to accelerate in pitch and roll directions by 1-5%, and has over 600% the yaw control of the conventional design, both with and without a rotor failure. Table 2 shows the gains of the new design in the lateral directions (x and y) with about an 5% gain in vertical acceleration.

When compared to a DFC *X6*, the *Y6sC* has a higher roll rate capability due to the the inertia differences, as long as the motor mounts are lighter in inertia than the arms are. The rate differential is limited because the inertia isn't actually halved

Table 1. Calculated maximum angular rates *Y6sC* (ζ = 30°) vs conventional *Y6C* (ζ = 0°) for a 4S 5" rotor vehicle. Single rotor (M1 Figure 3) fault data are included.

	$+\dot{p}, -\dot{p}$	$+\dot{q}, -\dot{q}$	$+\dot{r}, -\dot{r}$ $(°/s^2)$
Y6C	714,-714	607,-607	38,-40
Y6sC	749,-736	630,-624	276,-306
% difference	+5,+3	+4,+3	+629,+674
Y6C M1 out	714,-327	449,-607	39,-40
Y6sC M1 out	749,-331	466,-624	275,-160
% difference	+5,+1	+4,+3	+611,+306

Table 2. Calculated maximum linear rates *Y6sC* (ζ = 30°) vs conventional *Y6C* (ζ = 0°) for a 4S 5" rotor vehicle, ζ = 30°. Single rotor (M1 Figure 3) fault data are included.

	$+\dot{x}, -\dot{x}$	$+\dot{y}, -\dot{y}$	$-\dot{z}$ (ft/s^2)
Y6C	-	-	-107
Y6sC	21,-20	21,-26	-112
% difference	-	-	+5
Y6C M1 out	-	-	-81
Y6sC M1 out	9,-20	21,-19	-85
% difference	-	-	+5

when considering extra mount equipment and the moment is slightly smaller in the *Y6sC* case due to the semi-coaxial rotors. In the yaw direction, the *Y6sC* wins again with about 50% more authority. This difference drops by about 15% when aerodynamic effects are considered, using data acquired on the thrust stand.

Any rotor faults on the *Y6C* are detrimental to the pure motion design space. When *M1* is faulted on the *Y6sC*, half of the design space for pure roll is taken out. However, the *Y6sC* with a faulted rotor does better for pure motion in roll, pitch than *Y6C* with no faults at most any values of ζ, ε although many solutions are not found, especially in roll.

THRUST STAND RESULTS

Thrust stand A thrust stand was designed and constructed to assist the investigation of the questions around semi-coaxial efficiency. The thrust stand is capable of measuring thrust, independent torque, current, voltage measurements from two rotors in customizable configurations. The stand is seen in Figure 6.

This system minimizes undesired ground/ceiling effects associated with more simple, low-clearance, vertically mounted stands, and allows for multiple motors in multiple coaxial, semi-coaxial, and coplanar configuration. The pivot point in the bottom of the stand largely eliminates non-axial moments, passing essentially only the moment created by thrust to the Uxcell 5 kg load cell, which measures overall thrust. Two independent load cells are mounted against two more independent motor mounts, which are free to rotate on bearings around each rotor's rotation axis. These mechanisms allow for aerodynamic torque measurement of each motor independently. Turnigy 2836\8 1100 K_v brushless motors were

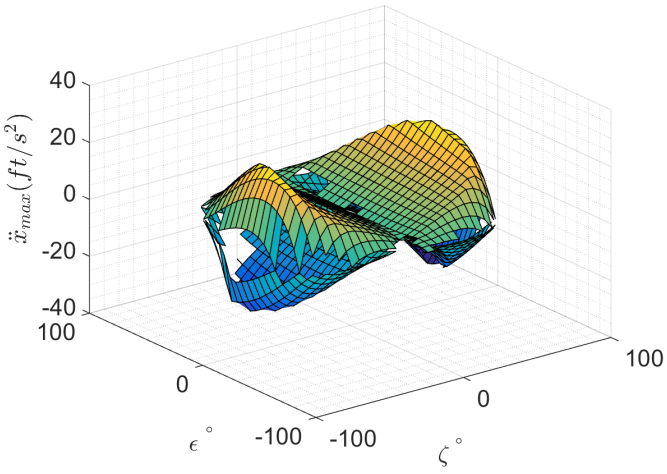

Fig. 5. *Y6sC* $\ddot{x}$ design space, pure motion enforced, co-rotating, no rotor faults

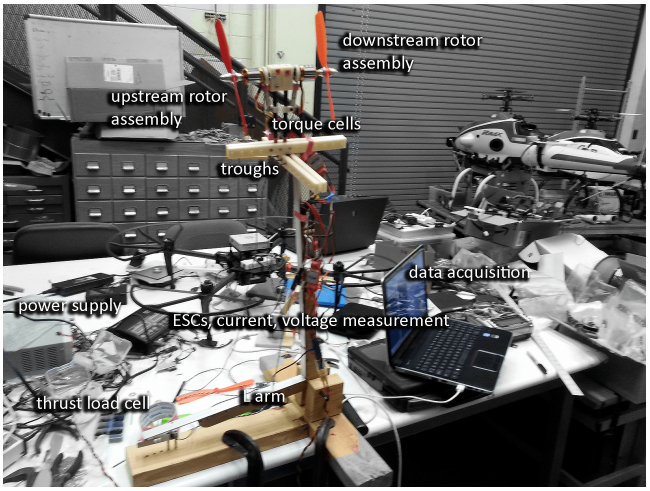

Fig. 6. Adjustable thrust stand (foreground) to measure thrust, independent torque, current, voltage

mounted on bearings inside a sleeve, which had protruding screws, mounted 45° from each other. For torque measurement for each motor, a Uxcell 0.1 kg load cell was centered without contact between the two screws on the rotating disc to measure torque once the motor started spinning. This allows the cell to measure torque in both directions so that the stand does not have to be physically modified once the rotor direction is inverted. Of course, the three wires hanging from the motor add a non-negligible restoring moment, so torque measurements would need to be calibrated for more accurate values of torque. However, since the motor bearing sleeve is only free rotate less than 15°, this undesirable restoring moment should be small compared to the aerodynamic torque. Also, this study is more focused on relative effect of configuration changes. Data are compared to the database released by Brandt (Ref. 25) to ensure readings are of the correct order. The rotor, arm coupler, bearing/sleeve, and carbon arm form the arm/rotor assembly.

Long, 3D-printed brackets with motor assembly troughs (seen

in Figure 6) and screw holes were mounted on top of the L-arm. The whole arm/rotor assembly was then mounted through a rectangular, pressed fit bracket to a rod that could be independently moved along the cutouts at the top of the L. Two of these assemblies were made so that coaxial and coplanar motor orientation cases could be tested. HX711AD modules were used to read the load cell voltages. Using this set up in tandem with variable brackets, each motors orientation, spin direction and attached propeller (8x4.5 GWS) could be altered independently. This was particularly useful to discern noticeable changes in performance between co-rotating and counter-rotating coaxial rotor cases in several different orientations. A 600 W bench power supply set to 12 V was connected to a parallel voltage sensor, then through two Turnigy 30 A Plush electronic speed controllers (ESCs) and a receiver. The ESCs were then each connected in series to separate inline ACS712 current sensors, and connected to the motors. The voltage sensor, the two current sensors for motor 1 (upstream, when applicable) and motor 2 (downstream, when applicable), the torque load cells and thrust load cell were each connected to separate analog input pins in an Arduino Pro Mini board. This board was connected through the serial port to the computer, which could then calibrate and record the values for each sensor. The Parallax Data Acquisition tool (PLX-DAQ), an Microsoft Excel-based serial monitor client, was then used to open the Arduino serial stream to record sensor data.

Several motor and stand orientation cases were used to analyze the relative thrust performance and efficiency these configurations: fully coaxial, semi-coaxial, co- and counter-rotating cases with differing separation distances (measured relative to the center of each propeller's hub), ground and ceiling effects on a single rotor at different clearances, and coplanar angled cases with both co- and counter-rotation at a fixed separation distance. Each trial consisted of changing the motor positioning along the bracket, starting the data acquisition, and adjusting the RPM of each rotor to 3000 after calibration. This ensured repeatability of the results and an accurate measure of thrust that would be comparable between orientations.

Coaxial and semi-coaxial rotors The coaxial configuration is commonly used in multirotor design. This has inspired a closer investigation into coaxial rotors at this scale. Two rotors are mounted on an adjustable bracket as seen in Figure 7.

While coaxial, the motors had varying separation distances from 1.8 inches to 13.6" hub to hub, corresponding to diameter-nondimensionalized values s_D of 0.23 to 1.7. The separation distance affects efficiency similarly to ζ because with non-zero ζ, inter-rotor wash effects are diminished. The data recorded is shown in Figure 8.

Since the wake of the upstream rotor contracts, as described by momentum theory, it effects less area of the downstream rotor. This might reduce the interference power loss. However, the freestream velocity ingested by the downstream rotor also increases, which also has the effect of increasing torque

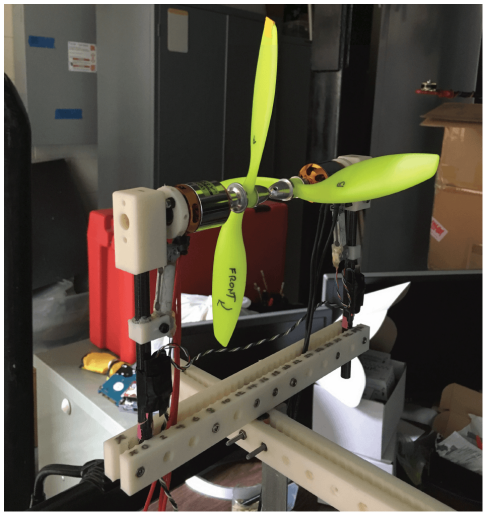

Fig. 7. Thrust stand configuration for coaxial rotors

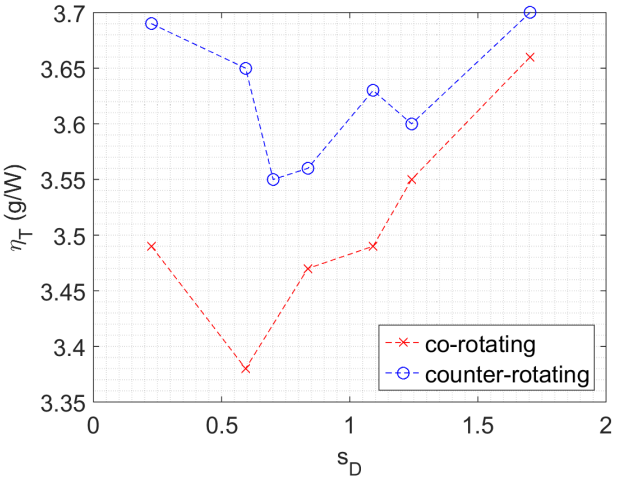

Fig. 8. Propulsive efficiency η_T of co- vs. counter-rotating coaxial rotors at different hub-hub separations s_D

on the downstream rotor. An average thrust of 76.4 g (co-rotating) and 81.7 g (counter-rotating) was found for these test conditions (i.e., 12 V and 3000 RPM for both motors 1 and 2), indicating the counter-rotating configuration suffers less thrust loss than the co-rotating configuration when coaxially mounted (as compared to two independently mounted rotors). The counter-rotating configuration appears to be more efficient for essentially all values of s_D; this counter-rotating coaxial configuration was found to be from about 1 to 6% more efficient. When stacking rotors in this configuration, almost no difference was seen in the upstream rotor's mechanical or electrical power, confirming the results found in (Ref. 22). A side benefit of the counter-rotating coaxial case is the reduction of high-speed retreating blade stall as compared to the co-rotating case due to the increase in tangential velocity seen by the downstream propeller. In the co-rotating case, aerodynamic steady state torque of the downstream rotor increased by up to 25%. A noticeable amount of additional vibration was observed in the co-rotating case, indicating high

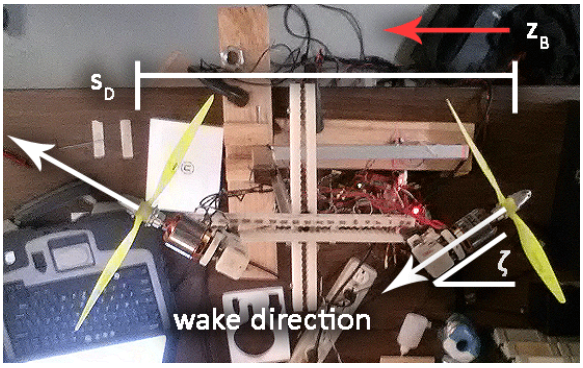

Fig. 9. Semi-coaxial configuration on thrust stand. Both rotors spin such that the wake airflow is aimed generally to the left, producing thrust generally to the right.

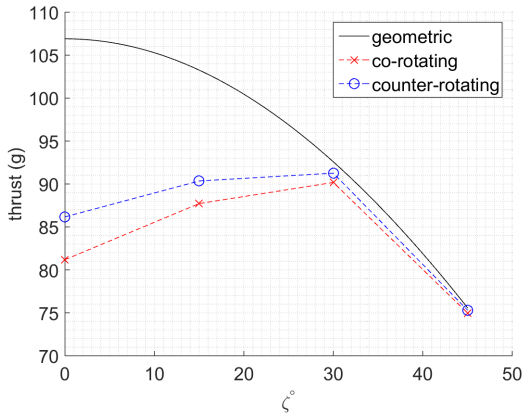

Fig. 10. Semi-coaxial configuration (s_D = 0.71) expected thrust in response to geometric angle compared to measured thrust including inter-rotor aerodynamics. Semi-coaxial configuration at 30° produces more thrust than the coaxial configuration at 0°, all else being equal.

levels of turbulence.

The configuration where rotors are mounted in a semi-coaxially is shown in 9. It is seen from Figure 10 that near $\zeta = 30°$, thrust achieved is nearly that which is expected at that rotor geometry. The geometric, expected thrust is the thrust that would be expected in the $-z_B$ axis (as if these are mounted on a multirotor arm) ignoring aerodynamics interactions between the two rotors. That is, the base value of the geometric thrust at $\zeta = 0°$ is the sum of the upstream rotor's thrust when the downstream rotor is off, and vise versa. In other words, the geometric thrust is the independent rotor thrust summed of both motors gathered at zero ζ with no aerodynamic effects, then scaled by $sin(\zeta)$. At low ζ the aerodynamic effects are a major as seen in Figure 10. At around 40° the results begin to align against the geometric where no aerodynamic effects are considered. Note that the thrust generated with ζ around 30° generates more thrust than what was gained by either co/counter rotating props at zero ζ.

This geometric expected thrust in the equivalent of $-z_B$ ignoring wake effects is equivalent to what is observed near $\zeta = 30°$ and beyond on the thrust stand. This is indicates that the wake of the upstream rotor is no longer affecting the downstream rotor. Note from the figure that as ζ increases (i.e., the rotors become less coaxial), efficiency in thrust in $-z_B$ *also increases*. This must be a function of the specific rotors and their RPM but these data serve to illustrate the point that semi-coaxial rotors *still* outperform coaxial ones in thrust in $-z_B$, even though they are rotated away from the $-z_B$ axis, which serves to geometrically decrease thrust in that direction. As in the coaxial trials, the counter-rotating configuration appears to be more efficient. This is also seen in the figure at $\zeta = 0°$.

Note the 19% loss in thrust at $\zeta = 0°$ (coaxial) configuration for counter-rotating rotors and the 24% loss for co-rotating rotors. The difference between the two disappears as the upstream wake rotates away from the downstream rotor.

FLIGHT TEST RESULTS

A prototype of the *Y6sC* configuration is built and flown to test predicted performance calculations. The vehicle features an adjustable motor mount system which allows motor tilt ζ to be adjusted on both the top and bottom set of rotors. The vehicle is flown with four different ζ values: 0° (i.e., conventional coaxial), and 15°, 25°, and 35° (i.e., semi-coaxial configurations).

Autopilot configuration

For initial testing purposes to validate the new design, a Pixhawk autopilot (Ref. 26) was used. The Pixhawk is a common, open-source hardware/software project used by hobby drone enthusiasts. Research platoforms have also successfully employed Pixhawks, an example being Georgia Tech's autonomous first place finish (Ref. 28) developed for the AHS micro aerial vehicle (MAV) challenge in 2015. Custom firmware was written to allow for DFC capability.Standard mode II joystick controls are used: left stick throttle and yaw rate and right stick controls roll and pitch. To be able to fully utilize the new degrees of freedom, a new control method was developed. The DFC mode has the Pixhawk perform attitude control using a standard proportional-integral-derivative (PID) design freeing up the right stick for DFC (body acceleration) control. The right stick commands in DFC mode became body x and y acceleration. Trim knob functionality was added to allow for hovering at non-zero attitudes, the calculated maximums of which are shown in Figures 12, 13, and 14. Since the vehicle is not symmetric, the maximum trim angle is not equivalent in the positive and negative pitch directions. Note also that the practical maximum without 3D rotors is around 10-20° in pitch because generally vehicles are designed to fly around 50% throttle (i.e., mg/T_{max}). An added benefit found from flying with this mode was that it is much easier for the safety pilot. No longer does the pilot need to worry about the attitude of the vehicle, which is helpful in certain situations. DFC mode flies similarly to a GPS mode where the pilot is only in control of position changes. Code was also added to allow for testing motor-out scenarios.

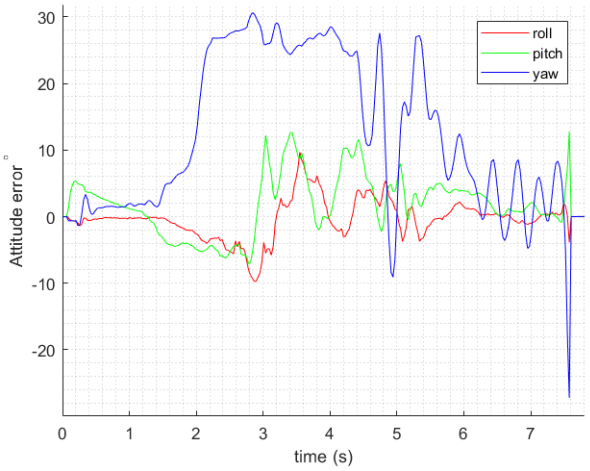

Fig. 11. Estimated error of *Y6sC* with failed rotor in flight

The controller would not have awareness of the motor-out but would have to adapt to the change. Figure 11 shows that the vehicle tracks attitude commands to a reasonable degree despite the lack of knowledge of a failed rotor; within about 10° in roll and pitch and 30° in yaw. It is possible to tune the yaw oscillations out if desired (yaw authority is too high and stock gains are used). An approximately 7 second portion of flight is shown. It is expected that these errors would shrink considerably with tuned gains and an adaptive controller.

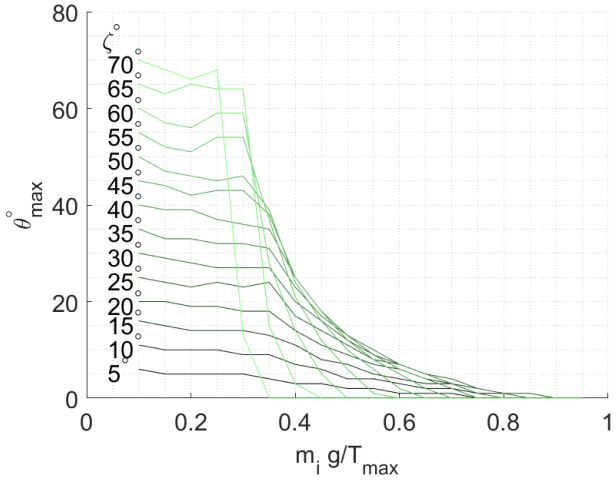

Fig. 12. Calculated maximum pitch during trimmed hover for *Y6sC* with hover throttle percentage

Flight testing

The vehicle is flown to qualitatively test the ability of the vehicle to hover and maneuver, but mainly to confirm efficiency enhancements seen in the thrust stand data. It is flown manually and hovered with a Pixhawk and current/voltage meter. Figure 15 shows the predicted loss of efficiency (based solely

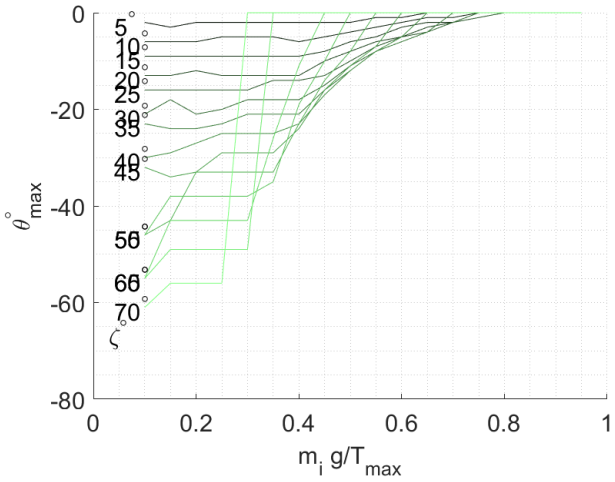

Fig. 13. Calculated minimum pitch during trimmed hover for *Y6sC* with hover throttle percentage

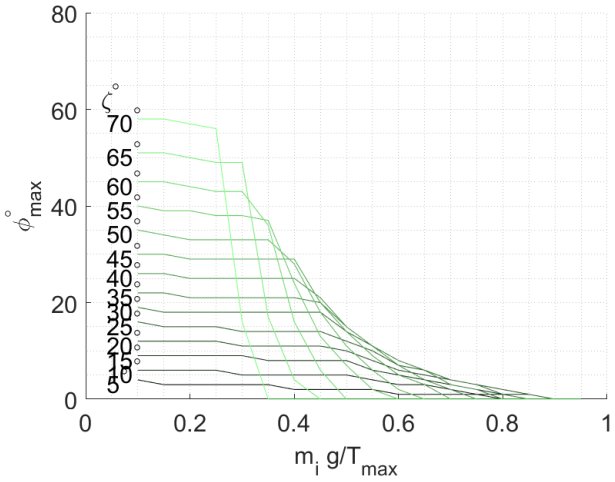

Fig. 14. Calculated maximum roll during trimmed hover for *Y6sC* with hover throttle percentage

on the geometry of the thrust vectors) is much higher than what is seen in flight test. Hover power data are recorded for several minutes for each configuration and then averaged. Note the slight increase in efficiency around $\zeta = 15°$, although note that this may be noise. In either case, even around 25° of motor tilt, electrical efficiency *is not reduced*. This indicates that DFC is essentially free for this configuration. Even at 15°, there is sufficient acceleration to handle "normal" disturbances and hold position more effectively than a conventional *Y6*.

The vehicle is also flown manually with one motor out (the propeller is removed). The controller is unaware of the failure. This is done to substantiate the output from the actuation authority framework described in the DFC simulation and optimization section. The vehicle retains the nearly-fully actuated ability that it has with all six rotors functioning. Note

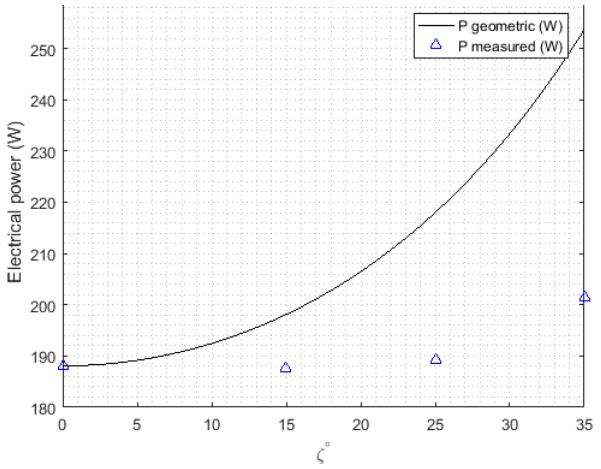

Fig. 15. Measured electrical hover power when *Y6sC* is flown at different motor tilt values compared to geometric-predicted hover power.

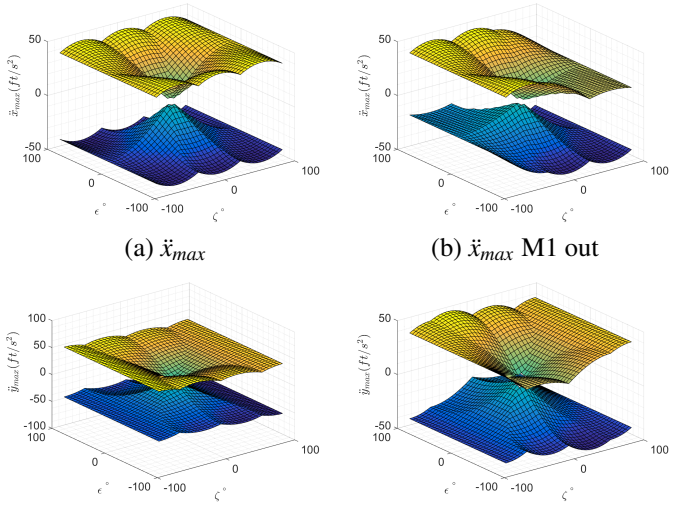

(a) $\ddot{x}_{max}$ (b) $\ddot{x}_{max}$ M1 out

(c) $\ddot{y}_{max}$ (d) $\ddot{y}_{max}$ M1 out

Fig. 16. *Y6sC* actuation authority with no faults (left) and motor M1 failed (right). Design variables motor tilt (ζ) and arm dihedral (ε)

that some of the directions become asymetric (with respect to positive and negative directions in the same axes) as seen in Figure 16. To the manual, human pilot, there is no noticeable effect of the one rotor out case.

CONCLUSION

This paper introduced the semi-coaxial multirotor, specifically the *Y6sC*, inspired by the conventional *Y6*. Design of the vehicle is described as well as advantages including free DFC and a more efficient hover. Rotor out cases are described and thrust stand data of the new configuration are shown. Flight test data are shown varying design parameter ζ of the configuration, including a rotor out flight.

REFERENCES

[1]Mulgaonkar, Y., Whitzer, M., Morgan, B., Kroninger, C. M., Harrington, A. M., and Kumar, V., "Power and weight considerations in small, agile quadrotors," Micro-and Nanotechnology Sensors, Systems, and Applications VI, Vol. 9083, 2014.

[2]Augugliaro, F., Mirjan, A., Gramazio, F., Kohler, M., and D'Andrea, R., "Building tensile structures with flying machines," Intelligent Robots and Systems (IROS), 2013 IEEE/RSJ International Conference on, 2013.

[3]Mellinger, D., Lindsey, Q., Shomin, M., and Kumar, V., "Design, modeling, estimation and control for aerial grasping and manipulation," Intelligent Robots and Systems (IROS), 2011 IEEE/RSJ International Conference on, 2011.

[4]Fumagalli, M., Naldi, R., Macchelli, A., Forte, F., Keemink, A. Q., Stramigioli, S., Carloni, R., and Marconi, L., "Developing an aerial manipulator prototype: Physical interaction with the environment," *IEEE robotics & automation magazine*, Vol. 21, (3), 2014, pp. 41–50.

[5]Gioioso, G., Ryll, M., Prattichizzo, D., Bülthoff, H. H., and Franchi, A., "Turning a near-hovering controlled quadrotor into a 3D force effector," Robotics and Automation (ICRA), 2014 IEEE International Conference on, 2014.

[6]Yüksel, B., Secchi, C., Bülthoff, H. H., and Franchi, A., "A nonlinear force observer for quadrotors and application to physical interactive tasks," Advanced Intelligent Mechatronics (AIM), 2014 IEEE/ASME International Conference on, 2014.

[7]"Cleandrone," http://www.cleandrone.com, Accessed: 06/19/2017.

[8]Jiang, G. and Voyles, R., "A nonparallel hexrotor UAV with faster response to disturbances for precision position keeping," Safety, Security, and Rescue Robotics (SSRR), 2014 IEEE International Symposium on, 2014.

[9]Jiang, G., Voyles, R., Sebesta, K., and Greiner, H., "Mockup of the exhaust shaft inspection by dexterous hexrotor at the DOE WIPP site," Safety, Security, and Rescue Robotics (SSRR), 2015 IEEE International Symposium on, 2015.

[10]Crowther, B., Lanzon, A., Maya-Gonzalez, M., and Langkamp, D., "Kinematic analysis and control design for a nonplanar multirotor vehicle," *Journal of Guidance, Control, and Dynamics*, Vol. 34, (4), 2011, pp. 1157–1171.

[11]Jiang, G. and Voyles, R., "Hexrotor uav platform enabling dextrous interaction with structures-flight test," Safety, Security, and Rescue Robotics (SSRR), 2013 IEEE International Symposium on, 2013.

[12]Kaufman, E., Caldwell, K., Lee, D., and Lee, T., "Design and development of a free-floating hexrotor UAV for 6-dof maneuvers," Aerospace Conference, 2014 IEEE, 2014.

[13]Rajappa, S., Ryll, M., Bülthoff, H. H., and Franchi, A., "Modeling, control and design optimization for a fully-actuated hexarotor aerial vehicle with tilted propellers," Robotics and Automation (ICRA), 2015 IEEE International Conference on, 2015.

[14]Nikou, A., Gavridis, G. C., and Kyriakopoulos, K. J., "Mechanical design, modelling and control of a novel aerial manipulator," Robotics and Automation (ICRA), 2015 IEEE International Conference on, 2015.

[15]Brescianini, D. and D'Andrea, R., "Design, modeling and control of an omni-directional aerial vehicle," Robotics and Automation (ICRA), 2016 IEEE International Conference on, 2016.

[16]Park, S., Her, J., Kim, J., and Lee, D., "Design, modeling and control of omni-directional aerial robot," Intelligent Robots and Systems (IROS), 2016 IEEE/RSJ International Conference on, 2016.

[17]Kiso, K., Ibuki, T., Yasuda, M., and Sampei, M., "Structural optimization of hexrotors based on dynamic manipulability and the maximum translational acceleration," Control Applications (CCA), 2015 IEEE Conference on, 2015.

[18]Polzin, K. A., Markusic, T. E., Stanojev, B. J., DeHoyos, A., and Spaun, B., "Thrust stand for electric propulsion performance evaluation," *Review of Scientific Instruments*, Vol. 77, (10), 2006, pp. 105108.

[19]Rand, O. and Khromov, V., "Aerodynamic optimization of coaxial rotor in hover and axial flight," 27th international Congress of the Aeronautical Sciences, 2010.

[20]Leishman, J. G. and Ananthan, S., "Aerodynamic optimization of a coaxial proprotor," Annual Forum Proceedings-American Helicopter Society, Vol. 62, 2006.

[21]Theys, B., Dimitriadis, G., Hendrick, P., and De Schutter, J., "Experimental and numerical study of micro-aerial-vehicle propeller performance in oblique flow," *Journal of Aircraft*, Vol. 54, (3), 2016, pp. 1076–1084.

[22]Otsuka, H. and Nagatani, K., "Thrust loss saving design of overlapping rotor arrangement on small multirotor unmanned aerial vehicles," Robotics and Automation (ICRA), 2016 IEEE International Conference on, 2016.

[23]Aleksandrov, D. and Penkov, I., "Optimal gap distance between rotors of mini quadrotor helicopter," Proceedings of the 8th DAAAM Baltic Conference, Tallinn, Estonia, 2012.

[24]Bershadsky, D., *Electric multirotor design and optimization*, Ph.D. thesis, Georgia Institute of Technology, 2017.

[25]Brandt, J. and Selig, M., "Propeller performance data at low reynolds numbers," 49th AIAA Aerospace Sciences Meeting including the New Horizons Forum and Aerospace Exposition, 2011.

[26]Team, A. D., "Ardupilot autopilot suite," *URL http://ardupilot.org/. Accessed*, 2016, pp. 05–20.

[27]Johnson, E. N. and Schrage, D. P., "System integration and operation of a research unmanned aerial vehicle," *AIAA Journal of Aerospace Computing, Information, and Communication*, Vol. 1, (1), 2004.

[28]Haviland, S., Bershadsky, D., Magree, D., and Johnson, E. N., "Development of a 500 gram Vision-based Autonomous Quadrotor Vehicle Capable of Indoor Navigation," , 2015.